Valley-selective optical Stark effect in monolayer WS₂

Edbert J. Sie[1], James W. McIver[1,2], Yi-Hsien Lee[3], Liang Fu[1], Jing Kong[4] and Nuh Gedik[1]*

Breaking space–time symmetries in two-dimensional crystals can markedly influence their macroscopic electronic properties. Monolayer transition metal dichalcogenides (TMDs) are prime examples where the intrinsically broken crystal inversion symmetry permits the generation of valley-selective electron populations[1-4], even though the two valleys are energetically degenerate, locked by time-reversal symmetry. Lifting the valley degeneracy in these materials is of great interest because it would allow for valley-specific band engineering and offer additional control in valleytronic applications. Although applying a magnetic field should, in principle, accomplish this task, experiments so far have not shown valley-selective energy level shifts in fields accessible in the laboratory. Here, we show the first direct evidence of lifted valley degeneracy in the monolayer TMD WS₂. By applying intense circularly polarized light, which breaks time-reversal symmetry, we demonstrate that the exciton level in each valley can be selectively tuned by as much as 18 meV through the optical Stark effect. These results offer a new way to control the valley degree of freedom, and may provide a means to realize new Floquet topological phases[5-7] in two-dimensional TMDs.

The coherent interaction between light and matter offers a means to modify and control the energy level spectrum of a given electronic system. This interaction can be understood using what is known as Floquet theory[8], which states that a Hamiltonian periodic in time has quasistatic eigenstates that are evenly spaced in units of the photon driving energy. The simplest example of this is given by a two-level atomic system in the presence of monochromatic light, which can be fully described by the semi-classical Hamiltonian

$$\hat{H}(t) = \hat{H}_0 + \hat{p}\mathcal{E}(t) \qquad (1)$$

where $\hat{H}_0$ is the equilibrium Hamiltonian describing a two-level atom with eigenstates $|a\rangle$ and $|b\rangle$, $\hat{p}$ is the electric dipole moment operator of the atom, and $\mathcal{E}(t) = \mathcal{E}_0\cos2\pi\nu t$ is the oscillating electric field of light with amplitude $\mathcal{E}_0$ and frequency ν. The perturbation term in the Hamiltonian contains a time-dependent factor $(\cos2\pi\nu t)$ that enables the coherent absorption of light by $|a\rangle$ to form the photon-dressed state $|a+h\nu\rangle$, and the stimulated emission of light by $|b\rangle$ to form another photon-dressed state $|b-h\nu\rangle$, as shown in Fig. 1a. Additional states $|a-h\nu\rangle$ and $|b+h\nu\rangle$, as well as higher-order terms, also arise in this situation, but we omit them from Fig. 1a for the sake of clarity. This semi-classical description is consistent with the fully quantized approach (Supplementary Information).

The series of photon-dressed states formed in this way are called the Floquet states, which can hybridize with the equilibrium states $|a\rangle$ and $|b\rangle$ through the electric field term $\mathcal{E}$ in equation (1). This hybridization often results in energy repulsion between the equilibrium and Floquet states, the physics of which is equivalent to the hybridization between two atomic orbitals by the Coulomb interaction to form the bonding and anti-bonding molecular orbitals in quantum chemistry. The interaction between the two states always results in a wider energy level separation, and the magnitude of the energy repulsion becomes more substantial if the states are energetically closer to each other. In our case, there are two such pairs of states shown in Fig. 1a denoted as $\{|a+h\nu\rangle, |b\rangle\}$ and $\{|a\rangle, |b-h\nu\rangle\}$ with identical energy difference of $\Delta = (E_b - E_a) - h\nu$. Through the simultaneous energy repulsion of these pairs, the optical transition between states $|a\rangle$ and $|b\rangle$ is shifted to a larger energy. This phenomenon is known as the optical Stark effect[9,10], and the corresponding energy shift (ΔE) is given by

$$\Delta E = \frac{\mathcal{M}_{ab}^2 \langle \mathcal{E}^2 \rangle}{\Delta} \qquad (2)$$

where $\mathcal{M}_{ab}$ is the polarization matrix element between $|a\rangle$ and $|b\rangle$, and $\langle \mathcal{E}^2 \rangle$ $(= \mathcal{E}_0^2/2)$ is the time-averaged value of the electric field squared, proportional to the light intensity (Supplementary Information). Owing to the tunability of this energy shift by changing either the light intensity or frequency, the optical Stark effect has been routinely employed in the study of atomic physics and to facilitate the cooling of atoms below the Doppler limit[11].

Similar effects have been encountered in solid-state systems, where the electronic states are in the form of Bloch bands that are periodic in momentum space. In the presence of monochromatic light, the Hamiltonian of crystalline solids becomes periodic in both space and time, which leads to the creation of Floquet–Bloch bands that repeat in momentum and energy. Floquet–Bloch bands were very recently observed for the first time on the surface of a topological insulator irradiated by mid-infrared light[12]. The optical Stark effect can also occur in solids through the interaction between photo-induced Floquet–Bloch bands and equilibrium Bloch bands[13]. So far, this effect has been reported in only a very limited number of materials, with Cu₂O (ref. 14), GaAs (refs 15–18) and Ge (ref. 19) semiconductors among the few examples.

Here we report the first observation of the optical Stark effect in a monolayer TMD WS₂. The recently discovered monolayer TMDs are two-dimensional crystalline semiconductors with unique spin–valley properties[1] and energetically degenerate valleys at the K and K′ points in the Brillouin zone that are protected by time-reversal symmetry. We demonstrate by using circularly polarized light that the effect can be used to break the valley degeneracy and
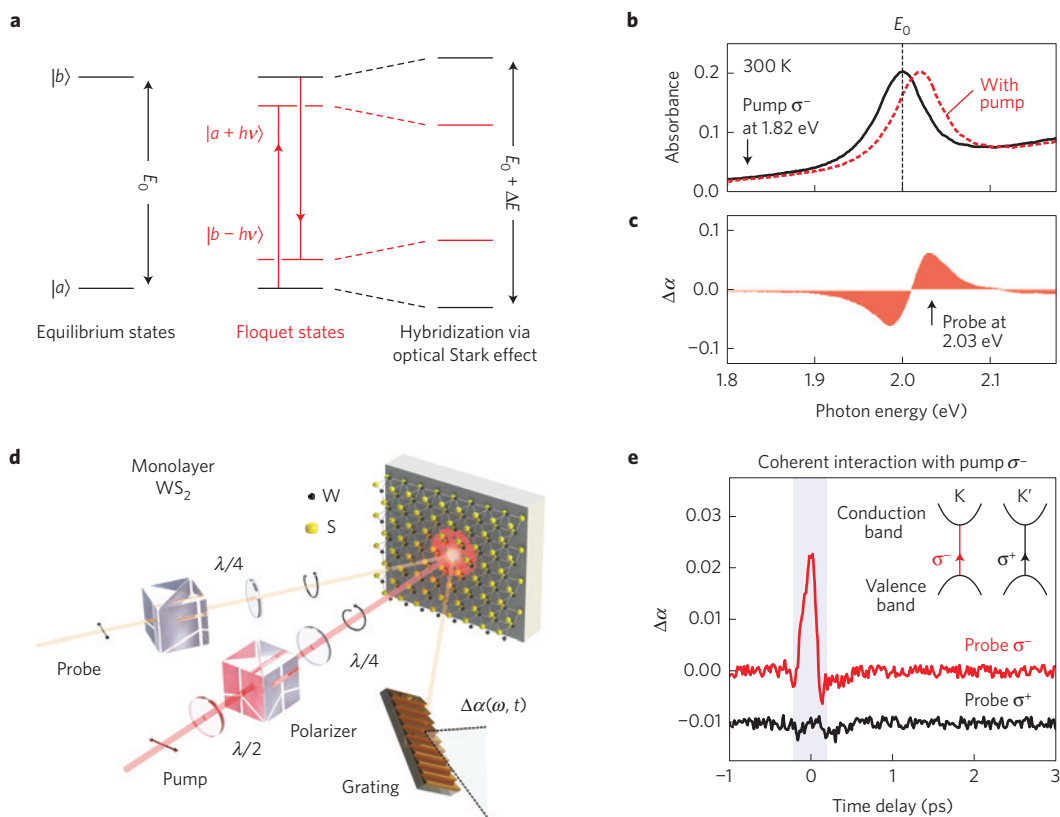
Figure 1 | The optical Stark effect and its observation in monolayer WS$_2$. a, Energy level diagram of two-level $|a\rangle$ and $|b\rangle$ atoms showing that the equilibrium and Floquet states $|a+h\nu\rangle$ and $|b-h\nu\rangle$ can hybridize, resulting in shifted energy levels. **b**, Measured absorbance of monolayer WS$_2$ (black) and a hypothetical absorbance curve (dashed) that simulates the optical Stark effect. **c**, The simulated change of absorption induced by the pump pulses. **d**, Schematic of transient absorption spectroscopy set-up (see Methods). **e**, Time trace of $\Delta\alpha$, induced by pump pulses of σ^- helicity, measured using probe pulses of the same (σ^-, red) and opposite (σ^+, black, with offset for clarity) helicities. It shows that the optical Stark effect occurs only during the pump pulse duration ($\Delta t = 0$ ps) and when the pump and probe helicities are the same.

raise the exciton level at one valley by as much as 18 meV in a controllable valley-selective manner.

In monolayer WS$_2$, the energy of the lowest exciton state is 2.00 eV at room temperature (Fig. 1b, black). To induce a sufficiently large energy shift of this exciton (as simulated and exaggerated for clarity in Fig. 1b, dashed), we use an optical parametric amplifier capable of generating ultrafast laser pulses with high peak intensity and tunable photon energy (1.68–1.88 eV). To measure the energy shift we use transient absorption spectroscopy[20] (Fig. 1d), which is a powerful technique capable of probing the resulting change in the absorption spectrum $\Delta\alpha$, as simulated in Fig. 1c (see Methods). The unique optical selection rules of monolayer TMDs allow for $\Delta\alpha$ at the K (or K') valley to be measured with valley specificity by using left (or right) circularly polarized probe light (inset in Fig. 1e).

To search for the optical Stark effect in WS$_2$, we start by measuring the change in the optical absorption $\Delta\alpha$ as a function of time delay Δt between the pump and probe laser pulses (Fig. 1e). To generate the necessary Floquet–Bloch bands, we tune the pump photon energy to 1.82 eV so that it is just below the absorption peak, with pulse duration 160 fs at full-width at half-maximum, fluence 60 μJ cm^{-2}, and polarization σ^- (left circularly polarized). As the optical Stark effect is expected to shift the absorption peak to higher energy, the probe photon energy is chosen to be 2.03 eV, which is above the equilibrium absorption peak. Figure 1e shows that when σ^- is used to probe $\Delta\alpha$ (red trace), there is a sharp peak that exists only at $\Delta t = 0$ ps when the pump pulse is present. This signifies that the measurement is sensitive to a coherent light–matter interaction occurring between the pump pulse and the sample. When σ^+ is used to probe $\Delta\alpha$ (black trace), we observe no discernible signal above

the noise level at all time delays. This shows that probing the optical Stark effect in this material is strongly sensitive to the selection of pump and probe helicities. Closer examination of the $\Delta\alpha$ spectrum in the range of 1.85–2.15 eV (Supplementary Information) reveals a faint but noticeable background signal that is present at both valleys. In the following discussion, we consider only results taken at $\Delta t = 0$ ps for which the background signals have also been subtracted to focus on the optical Stark effect (see Supplementary Information).

Having demonstrated that the optical Stark effect can be induced in a monolayer TMD, we now study its valley specificity and demonstrate that it can be used to lift the valley degeneracy. Figure 2a shows the $\Delta\alpha$ spectra induced by σ^- pump pulses probed in a valley-selective manner by using σ^- (K valley) and σ^+ (K' valley) probe helicities. When the same pump and probe helicities are used ($\sigma^-\sigma^-$, Fig. 2a left panel), the spectrum exhibits a positive (and negative) $\Delta\alpha$ at energy higher (and lower) than the original absorption peak $E_0 (= 2.00$ eV), clearly indicating that the absorption peak at the K valley is shifted to higher energy through the optical Stark effect. The spectrum of the opposite pump and probe helicities ($\sigma^-\sigma^+$, Fig. 2a right panel), in contrast, shows a negligible signal across the whole spectrum, indicating an insignificant change to the absorption peak at the K' valley. Figure 2c shows identical measurements of $\Delta\alpha$ using instead a σ^+ pump helicity, where it can be seen that the effect is switched to the K' valley. This valley-selective probing of the optical Stark shift shows that the effect is well isolated within a particular valley determined by the pump helicity. The magnitude of the effect in either valley can also be smoothly tuned as the pump helicity is continuously varied from fully σ^- to fully σ^+ (Supplementary Information).
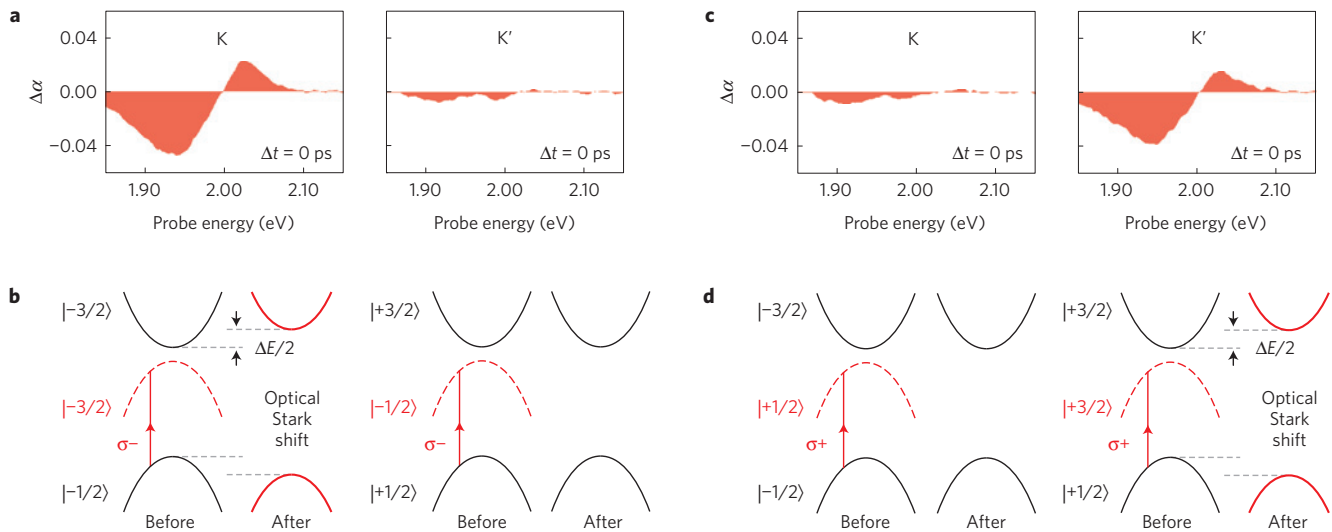
Figure 2 | The valley selectivity of the optical Stark effect. a, Valley-specific $\Delta\alpha$ spectra (background-subtracted) induced by σ^- pump pulses probed by using σ^- (K valley) and σ^+ (K′ valley) helicities. **b**, Band diagrams with the pump-induced Floquet–Bloch bands (red dashed curves) and their associated magnetic quantum numbers m. **c,d**, By switching the pump pulse helicity to σ^+, we also measured the valley-specific $\Delta\alpha$ spectra (**c**) and show their corresponding band diagrams (**d**). The optical Stark effect occurs only between states having the same magnetic quantum numbers.
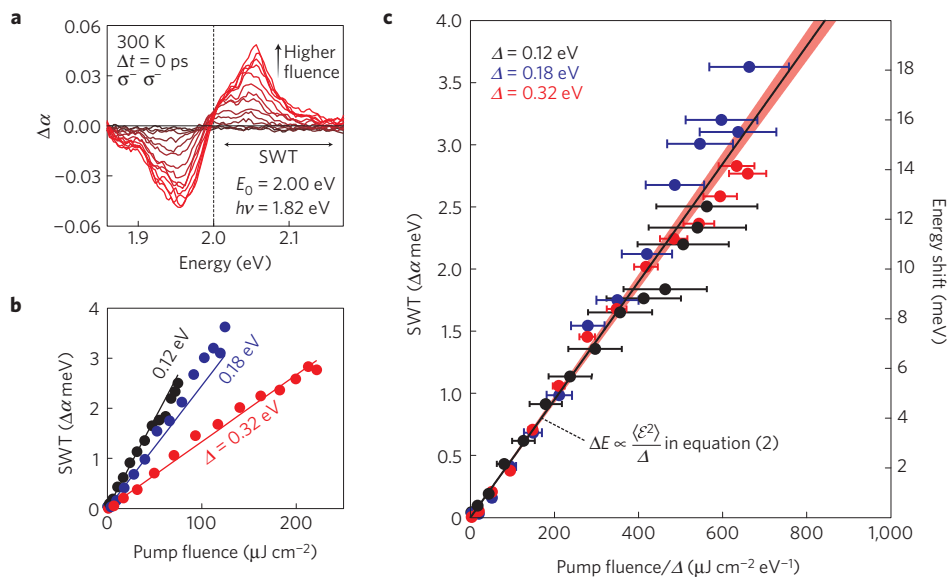
Figure 3 | Fluence and detuning dependences of the optical Stark shift. a, Fluence dependence of $\Delta\alpha$ spectra with fluences up to $120\,\mu\text{J cm}^{-2}$ measured with the same pump and probe helicities. **b**, Fluence and detuning dependences of the SWT with the integration range shown in **a**. **c**, SWT plotted as a function of fluence/Δ, showing that all of the data points fall along a common slope (black line). The horizontal error bars correspond to the pump bandwidth of 43 meV at full-width at half-maximum. The fitting slope (black line) and the 95% confidence band (red shading) shows an excellent agreement with the characteristic dependences of the optical Stark shift in equation (2).

The valley-specific optical Stark effect shares the same origin as the valley-selective photoexcitation that was previously reported in this class of materials[2–4]. Both effects arise owing to valley selection rules. In monolayer WS_2, the highest-occupied states in the valence band are associated with magnetic quantum numbers m, where $m = -1/2$ at the K valley and $+1/2$ at the K′ valley as shown in Fig. 2b and repeated in Fig. 2d. Meanwhile, the lowest-unoccupied states in the conduction band consist of four quasi-degenerate states, with $m = -3/2$ and $-1/2$ at the K valley, and $m = +3/2$ and $+1/2$ at the K′ valley. Two of these states ($m = \pm 1/2$) do not participate in the effect, and thus are omitted from the figures. Coherent absorption of light by the valence band (VB) creates a Floquet–Bloch band $|\text{VB} + h\nu\rangle$ for which the magnetic quantum number is added by the

light helicity that carries $\Delta m = -1$ (σ^-) or $+1$ (σ^+). The proximity in energy between this Floquet–Bloch band and the equilibrium conduction band can induce a hybridization that leads to an energy shift provided that they have the same magnetic quantum numbers. Although this material is known to possess a strong excitonic interaction, the physical description of the valley selectivity still remains the same and, for the purpose of understanding the effect, the energy of the equilibrium conduction band is essentially reduced by as much as the exciton binding energy[21]. This explains the valley-selective energy shift we observed in our experiments. These optical selection rules can be described by equation (2) after replacing $\mathcal{M}_{ab}$ by $\mathcal{M}_\nu$, which now represents the valley selection rules for different laser polarizations[21]. Additional experiments (below) investigating

the dependence on the light intensity and frequency show that the measured energy shift obeys equation (2) extremely well.

Figure 3a shows a series of $\Delta\alpha$ spectra that grow with increasing pump fluence. It can be shown (in Supplementary Information) that the integrated $\Delta\alpha$ as a function of energy, namely the spectral weight transfer (SWT), is proportional to the energy shift,

$$\int_{E_0}^{\infty} \Delta\alpha(\omega)\mathrm{d}\omega = A\Delta E \qquad (3)$$

where A is the peak absorbance of the sample. In our analysis, it is sufficient to integrate $\Delta\alpha$ in the range of $2.00 \leq \omega \leq 2.18$ eV because the signal vanishes beyond this upper limit. The SWT is plotted in Fig. 3b (blue circles) as a function of pump fluence, together with accompanying results measured with smaller (black) and larger (red) laser detuning energies Δ. Not only they show a linear dependence with fluence but they also share a common slope when plotted as a function of fluence/Δ in Fig. 3c. This is in excellent agreement with equation (2). By obtaining the peak absorbance $A = 0.2$ from Fig. 1c, and using equation (3) we can set an energy scale for ΔE in the right vertical axis of Fig. 3c, which estimates an energy shift of 18 meV measured at the highest fluence. We note that, for a given fluence and energy detuning, this material exhibits the largest optical Stark shift in any materials reported so far. We have used equation (2) to calculate the expected energy shift by using an estimated Rabi frequency, which agrees very well with the measured value (see Supplementary Information).

The ability to create valley-specific Floquet–Bloch bands in monolayer TMDs offers a means to induce new topological phases[5–7] with valley-specific edge states. To elucidate its valley specificity, we can ignore the excitonic interaction without loss of generality, and we conceive a situation where the σ⁻ detuning energy is varied across the interband transition, as shown in Fig. 4a (K valley) and b (K′ valley). In these figures, the coherent absorption of light (red line) from the valence band creates a Floquet–Bloch band close to the conduction band edge (dashed curves) and induces hybridization that results in energy repulsion (solid curves). When the pump detuning is set at $\Delta < 0$, band inversion should occur at the K′ valley, which is accompanied by an avoided crossing away from the symmetry point ($k = K' + \delta k$). This gap opening allows the creation of topological edge states (red)[22]. Here the pump helicity breaks time-reversal symmetry, inducing chiral edge states along the boundary of the laser-exposed region where the topological order changes (Fig. 4c)[23]. We note that this description is robust when the Floquet–Bloch band is far above the interband transition. In a situation where the photon energy approaches the exciton resonance, careful consideration of the excitonic effects is necessary especially within the Rabi splitting of the exciton–polariton energy dispersion[24]. In future works, it should be possible to investigate such Floquet chiral edge states provided that the probing signal is made insensitive to contributions from photoexcited excitons and intervalley scattering[25,26]. This opens an exciting avenue that merges Floquet-driven topological transition and valley physics together.

The observation of a large valley-selective optical Stark effect in monolayer WS₂ represents the first clear demonstration of broken valley degeneracy in a monolayer TMD. This is possible because of the formation of Floquet–Bloch states through the application of circularly polarized light, which breaks time-reversal symmetry and allows for the lifting of the intervalley spin degeneracy. These findings offer additional control for valley-switching applications on a femtosecond timescale, as well as providing a means to generate new valley-selective topological phases in monolayer TMDs.

Note added in proof: After the submission of this Letter we became aware of related studies on intervalley splitting by light[27] and magnetic field[28–31].
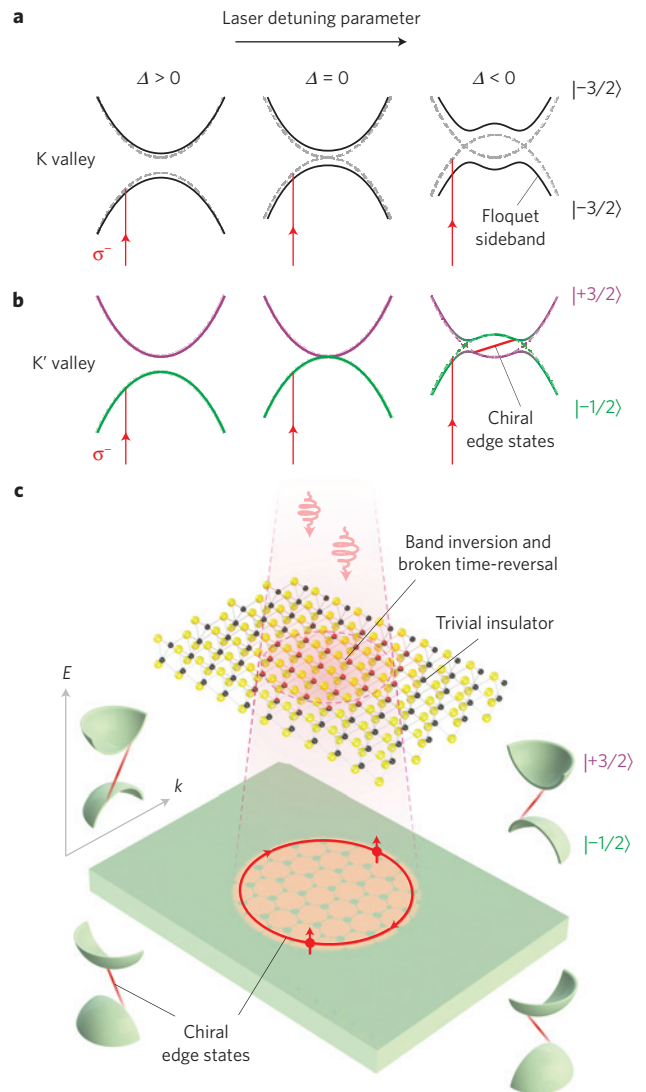

Figure 4 | Valley-specific Floquet topological phase. a,b, Hybridization between the Floquet–Bloch band and the conduction band when Δ is varied, which gives rise to the avoided crossing at the K valley (**a**) and the band inversion at the K′ valley (**b**). The crossing straight line (red) at the K′ valley is the anticipated chiral edge states due to the band inversion. **c,** Schematic of the Floquet-driven chiral edge state along the boundary of the laser-exposed region.

Methods

References

1. Xiao, D., Liu, G-B., Feng, W., Xu, X. & Yao, W. Coupled spin and valley physics in monolayers of MoS_2 and other group-VI dichalcogenides. *Phys. Rev. Lett.* **108,** 196802 (2012).
2. Mak, K. F., He, K., Shan, J. & Heinz, T. F. Control of valley polarization in monolayer MoS_2 by optical helicity. *Nature Nanotech.* **7,** 494–498 (2012).
3. Zeng, H., Dai, J., Yao, W., Xiao, D. & Cui, X. Valley polarization in MoS_2 monolayers by optical pumping. *Nature Nanotech.* **7,** 490–493 (2012).
4. Cao, T. *et al.* Valley-selective circular dichroism of monolayer molybdenum disulphide. *Nature Commun.* **3,** 887 (2012).
5. Inoue, J. & Tanaka, A. Photoinduced transition between conventional and topological insulators in two-dimensional electronic systems. *Phys. Rev. Lett.* **105,** 017401 (2010).
6. Kitagawa, T., Oka, T., Brataas, A., Fu, L. & Demler, E. Transport properties of nonequilibrium systems under the application of light: Photoinduced quantum Hall insulators without Landau levels. *Phys. Rev. B* **84,** 235108 (2011).
7. Lindner, N. H., Refael, G. & Galitski, V. Floquet topological insulator in semiconductor quantum wells. *Nature Phys.* **7,** 490–495 (2011).
8. Shirley, J. H. Solution of Schrodinger equation with a Hamiltonian periodic in time. *Phys. Rev.* **138,** B979–B987 (1965).
9. Autler, S. H. & Townes, C. H. Stark effect in rapidly varying fields. *Phys. Rev.* **100,** 703–722 (1955).
10. Bakos, J. S. AC Stark effect and multiphoton processes in atoms. *Phys. Rep.* **31,** 209–235 (1977).
11. Cohen-Tannoudji, C. N. & Phillips, W. D. New mechanisms for laser cooling. *Phys. Today* **43,** 33–40 (1990).
12. Wang, Y. H., Steinberg, H., Jarillo-Herrero, P. & Gedik, N. Observation of Floquet–Bloch states on the surface of a topological insulator. *Science* **342,** 453–457 (2013).
13. Joffre, M., Hulin, D., Migus, A. & Antonetti, A. Dynamics of the optical Stark effect in semiconductors. *J. Mod. Opt.* **35,** 1951–1964 (1988).
14. Fröhlich, D., Nöthe, A. & Reimann, K. Observation of the resonant optical Stark effect in a semiconductor. *Phys. Rev. Lett.* **55,** 1335–1337 (1985).
15. Mysyrowicz, A. *et al.* "Dressed excitons" in a multiple-quantum-well structure: Evidence for an optical Stark effect with femtosecond response time. *Phys. Rev. Lett.* **56,** 2748–2751 (1986).
16. Chemla, D. S. *et al.* The excitonic optical Stark effect in semiconductor quantum wells probed with femtosecond optical pulses. *J. Lumin.* **44,** 233–246 (1989).
17. Sieh, C. *et al.* Coulomb memory signatures in the excitonic optical Stark effect. *Phys. Rev. Lett.* **82,** 3112–3115 (1999).
18. Hayat, A. *et al.* Dynamic Stark effect in strongly coupled microcavity exciton polaritons. *Phys. Rev. Lett.* **109,** 033605 (2012).
19. Koster, N. S. *et al.* Giant dynamical Stark shift in germanium quantum wells. *Appl. Phys. Lett.* **98,** 161103 (2011).
20. Sie, E. J., Lee, Y-H., Frenzel, A. J., Kong, J. & Gedik, N. Biexciton formation in monolayer MoS_2 observed by transient absorption spectroscopy. Preprint at http://arxiv.org/abs/1312.2918 (2013).
21. Combescot, M. Optical Stark effect of the exciton. II. Polarization effects and exciton splitting. *Phys. Rev. B* **41,** 3517–3533 (1990).
22. Bernevig, B. A., Hughes, T. L. & Zhang, S. C. Quantum spin Hall effect and topological phase transition in HgTe quantum wells. *Science* **314,** 1757–1761 (2006).
23. Perez-Piskunow, P. M., Usaj, G., Balseiro, C. A. & Torres, L. E. F. F. Floquet chiral edge states in graphene. *Phys. Rev. B* **89,** 121401(R) (2014).
24. Liu, X. *et al.* Strong light–matter coupling in two-dimensional atomic crystals. Preprint at http://arxiv.org/abs/1406.4826 (2014).
25. Mai, C. *et al.* Many-body effects in valleytronics: Direct measurement of valley lifetimes in single-layer MoS_2. *Nano Lett.* **14,** 202–206 (2014).
26. Mai, C. *et al.* Exciton valley relaxation in a single layer of WS_2 measured by ultrafast spectroscopy. *Phys. Rev. B* **90,** 041414(R) (2014).
27. Kim, J. *et al.* Ultrafast generation of pseudo-magnetic field for valley exciton in WSe_2 monolayers. Preprint at http://arxiv.org/abs/1407.2347 (2014).
28. MacNeill, D. *et al.* Valley degeneracy breaking by magnetic field in monolayer $MoSe_2$. Preprint at http://arxiv.org/abs/1407.0686 (2014).
29. Aivazian, G. *et al.* Magnetic control of valley pseudospin in monolayer WSe_2. Preprint at http://arxiv.org/abs/1407.2645 (2014).
30. Srivastava, A. *et al.* Valley Zeeman effect in elementary optical excitations of a monolayer WSe_2. Preprint at http://arxiv.org/abs/1407.2624 (2014).
31. Li, Y. *et al.* Valley splitting and polarization by the Zeeman effect in monolayer $MoSe_2$. Preprint at http://arxiv.org/abs/1409.8538 (2014).
32. Lee, Y-H. *et al.* Synthesis of large-area MoS_2 atomic layers with chemical vapor deposition. *Adv. Mater.* **24,** 2320–2325 (2012).
33. Lee, Y-H. *et al.* Synthesis and transfer of single-layer transition metal disulfides on diverse surfaces. *Nano Lett.* **13,** 1852–1857 (2013).
34. Gutiérrez, H. R. *et al.* Extraordinary room-temperature photoluminescence in triangular WS_2 monolayers. *Nano Lett.* **13,** 3447–3454 (2012).

Author contributions

E.J.S. performed the experiments and the data analysis, and wrote the manuscript with crucial inputs from J.W.M., L.F. and N.G. The Floquet topological phase in TMDs was initially proposed by L.F. The monolayers of WS_2 were synthesized by Y-H.L., supervised by J.K. This project is supervised by N.G.

Additional information

Supplementary information is available in the online version of the paper. Reprints and permissions information is available online at www.nature.com/reprints. Correspondence and requests for materials should be addressed to N.G.

Competing financial interests

The authors declare no competing financial interests.